Theoretical study of Rb2 in He(N): potential energy surface and Monte Carlo simulations.

Grégoire Guillon, Alexandre Zanchet, Markku Leino, Alexandra Viel, Robert E Zillich

Theoretical study of Rb_2 in He_N: potential energy surface and Monte Carlo simulations

Grégroire Guillon,[†] Alexandre Zanchet,[†,¶] Markku Leino,[†] Alexandra Viel,[*,†] and Robert E. Zillich[*,‡,†]

Institut de Physique de Rennes, UMR 6251, CNRS & Université de Rennes I, F-35042 Rennes, France, and Institute for Theoretical Physics, Johannes Kepler Universität Linz, Altenbergerstraße 69, A-4040 Linz, Austria

E-mail: alexandra.viel@univ-rennes1.fr; robert.zillich@jku.at

[*]To whom correspondence should be addressed
[†]Institut de Physique de Rennes, UMR 6251, CNRS & Université de Rennes I, F-35042 Rennes, France
[‡]Institute for Theoretical Physics, Johannes Kepler Universität Linz, Altenbergerstraße 69, A-4040 Linz, Austria
[¶]Current address: Insituto de Física Fundamental, C.S.I.C., Serrano 123, 28006 Madrid, Spain

Abstract

An analytical potential energy surface for a rigid Rb_2 in the $^3\Sigma_u^+$ state interacting with one helium atom based on accurate *ab initio* computations is proposed. This 2-dimensional potential is used, together with the pair approximation approach, to investigate Rb_2 attached to small helium clusters He_N with $N = 1,2,3,4,5,6,12$ and 20 by means of quantum Monte Carlo studies. The limit of large clusters is approximated by a flat helium surface. The relative orientation of the dialkali axis and the helium surface is found to be parallel. Dynamical investigations of the pendular and of the in-plane rotation of the rigid Rb_2 molecule on the surface are presented.

Introduction

By their quantum nature and weak interaction with dopants, superfluid helium nanodroplets are "ultimate spectrocopic matrices"[1] allowing for the powerful HENDI (helium nanodroplet isolation) spectroscopy[2,3] of various species. Within the large variety of molecular dopants studied, alkali dimers have been the subject of many experimental and theoretical works.[4–20] Different experimental approaches varying from LIF absorption spectra, emission spectra, magnetic-circular-dichroism and pump-probe are used to study Li_2, Na_2, K_2, Rb_2 and Cs_2 attached to the surface of He_N.

One of the particularities of the alkali dimers and clusters attached to the helium droplets is the enrichment of high-spin species.[7] Indeed, alkali-metal atoms in their ground electronic state, when picked up by a beam of helium nanodroplets, remain on the helium surface as a consequence of the weaker helium alkali interaction than the helium-helium one. There, they can surf on the surface and eventually form dimers in helium-controlled cold collisions. Both triplet and singlet electronic states are accessible. However given the stronger binding in the singlet state, the formation of alkali dimers in the singlet state provokes significant size reduction of the clusters by evaporation, and detachment of the alkali dimer from the droplets. The energy release on the high spin triplet state formation is smaller and the alkali dimers are more likely to stay attached to a helium cluster.

In this way, helium cluster isolation spectroscopy becomes a perfectly adapted tool for the study of high-spin states of alkali molecules.[7,21,22]

The rubidium dimers in their ground triplet state $^3\Sigma_u^+$ attached to He_N have been experimentally studied by Ernst's group,[8,10,13,19] and Stienkemeier's group.[17,22] The high-spin selectivity induced by the ultracold bath of helium atoms indeed facilitates spectroscopic probing of the triplet state.

In the gas phase, rubidium dimers in various singlet states of both gerade and ungerade symmetry have been the subject of high resolution spectroscopic investigations by the group of Amiot.[23–27] With the achievement in 1995 of Bose-Einstein condensation of bosonic alkali atoms,[28–30] interest in the triplet state is rising.[31–35] Indeed, in this ultra-cold context, alkali dimers are formed by magnetic Feshbach resonance tuning, or as the product of photoassociation between laser precooled alkali atoms in atomic magneto-optical traps.[36] In typical traps, the alkali atoms are spin polarized and therefore high-spin alkali dimers (triplet state) are obtained.

On the theoretical side, however, there is still a huge demand of accurate calculations of structural and dynamic properties. At the *ab initio* level, the interaction potential curves of Rb_2 are are difficult to converge. Yet the precise description of Rb_2 potential curves is useful to better understand and predict the dynamics of molecular formation. To our knowledge, the lowest triplet state of Rb_2 was first fully calculated along with many other excited states by Spiegelmann *et al.*,[37] with the use of relativistic effective core pseudo potentials, including core-valence corrections. Quickly afterwards, two potential energy curves were obtained for the triplet ground state by Krauss[38] and then by Foucrault.[39] Both modified the initial view of the 1989 paper. In 2006, Lozeille *et al.*,[40] proposed a triplet state using the CIPSI package. More recently, a relativistic configuration interaction valence bond method was used to obtain the splitting between the 0_u^- and 1_u components of the ground triplet state of Rb_2.[41] Finally, a very recent triplet curve for Rb_2 has been published a few months ago by Soldán.[42] In this work dedicated to the lowest quartet state of the Rb_3 potential, a very recent effective relativistic small core potential has been used. Beside *ab initio* calculations, an alternative way to get accute alkali dimer potential curves has been brought by the ultra-cold community. It relies on fitting a Born-Oppenheimer curve to various spectroscopic, including hy-

perfine structure, and collisional data. Such scheme has been used last year to optimize the triplet Rb_2 curve.[43]

In addition to the dimer potential, the question of the accurate description of the interaction between a rubidium and a helium atom is still open. Diatomic potentials by Pascale[44] have been used for a long time for the study of processes occuring in thermal collisions between ground or excited alkali atoms and helium atoms. More accurate ground state curves have been obtained by Kleinekathöfer *et al.*[45] for very weakly bound van der Waals systems, including heavy alkali atoms. More recent potentials for ground and excited states for all alkali-helium interactions, calculated by a relativistic DFT method and including spin-orbit effects, have been published by Zbiri *et al.*[46] But still, and quite generally, the theoretical computation of the correlation energy, so important to describe properly medium and long range parts of the ultra-weak alkali-helium interaction, is out of sight nowadays at least for full-electron calculations for heavy atoms. Pseudopotentials and polarization potentials, calibrated on atomic properties, have to be employed.

In the present paper, we report diffusion and path integral quantum Monte Carlo studies of the rubidium dimer in its ground triplet state in a helium environment. To this end, we first describe the *ab initio* calculations and detail the analytical fitting of the potential energy surface between a rigid Rb_2 dimer and a helium atom. After a short paragraph on the theoretical approaches, we present results obtained for small clusters with up to 20 helium atoms, followed by the case of a rubidium dimer attached to a helium film taken as the limit of the surface of larger droplets. We present in particular the study of the influence of the helium atoms on the rotational motion of the Rb_2 dimer.

Rb_2-He interaction potential

ab initio calculations

The interaction between a rigid Rb_2 and a He atom is computed using high level *ab initio* calculations. The first triplet state $1^3A'$ of the Rb_2He system is obtained using the restricted Hartree-Fock

calculation followed by a single-reference restricted open-shell coupled cluster method with single, double and noniterative triple excitations [RCCSD(T)]. The counter-poise correction of Boys and Bernardi[47] is applied to the interaction energies between He and Rb_2 in order to compensate for the basis set superposition errors. The Rb_2 equilibrium distance of 6.118 Å is used. All the *ab initio* calculations are performed using the MOLPRO 2006.1 package.[48] Following the quality test studies performed on Rb_2 by Pavel Soldán,[42] 9 valence electrons ($4s^2 4p^6 5s^1$) and the relativistic core potential ECP28MDF[49] to describe the inner electrons are used for the description of the two rubidium atoms. The basis set referred to as **B** in Ref. 42, which compares better with experiments for the diatomic contants of Rb_2, is employed for the 9 valence electrons. It is composed of 123 primitive Gaussian functions (13s,10p,5d,3f,1g) per Rb atom augmented by a set of diffuse functions (1s,1p,1d,1f,1g). The uncontracted d-aug-cc-pV5Z basis set limited to *spdf*, thus with 78 primitive fuctions, is used for the description of the helium atom.

As detailed in Ref. 42, using the above basis sets, the Rb_2 triplet state minimum is obtained at 6.118 Å with a well depth of $D_e = 240.9$ cm^{-1} which are in good agreement with the experimental ones, $r_e = 6.069$Å and $D_e = 241.45$ cm^{-1}.[50] The HeRb diatomic potential presents an equilibrium distance of 7.42 Å and a well depth of 0.934 cm^{-1}. The more stable configuration of the triatomic Rb_2-He system occurs for a T-shape geometry with a Rb_2 distance equal to 6.118 Å and with the He atom distant of 6.30 Å from the Rb_2 center of mass. The energy of this geometry is 2.60 cm^{-1} below that of the separated Rb_2 and He moities.

Analytical potential energy surface

The Rb_2He system is described using the Jacobi coordinates R, γ, where R is the distance between the He atom and the center of mass of Rb_2 and γ the angle between R and the Rb_2 molecular axis. In our notation, $\gamma = 0$ corresponds to the linear geometry, while $\gamma = \pi/2$ to the T-shape configuration. The global fit of the potential energy interaction for Rb_2He is based on the RKHS interpolation method.[51] It relies on 108 *ab initio* points sampling a regular two-dimensional grid. The grid contains the four angles values $\gamma = 0; \pi/4; 3/8\pi$ and $\pi/2$ for 27 R distances sampling

more densely the region of the potential well.

The two-dimensional potential function is given by

$$V_{Rb_2He}(R,\gamma) = \sum_{i=1}^{N_R}\sum_{j=1}^{N_\gamma} \alpha_{ij} q_1^{n_x,m}(x_i,x) q_2^{n_y}(y_j,y), \tag{1}$$

where $q_1^{n,m}$ and q_2^n are respectively distance-like and angle-like reproducing kernels as detailed in Ref. 51. In the above equation, the reduced coordinates

$$x = R^2 \tag{2a}$$

$$y = \sin(\gamma), \tag{2b}$$

such that $x \in [0,\infty]$ and $y \in [0,1]$, have been used. The three parameters n_x, n_y and m are all taken equal to 2 to insure a smooth interpolation and the correct asymptotic behaviour.

The resulting two dimensional RKHS potential is shown in Figure 1. As it can be seen, the

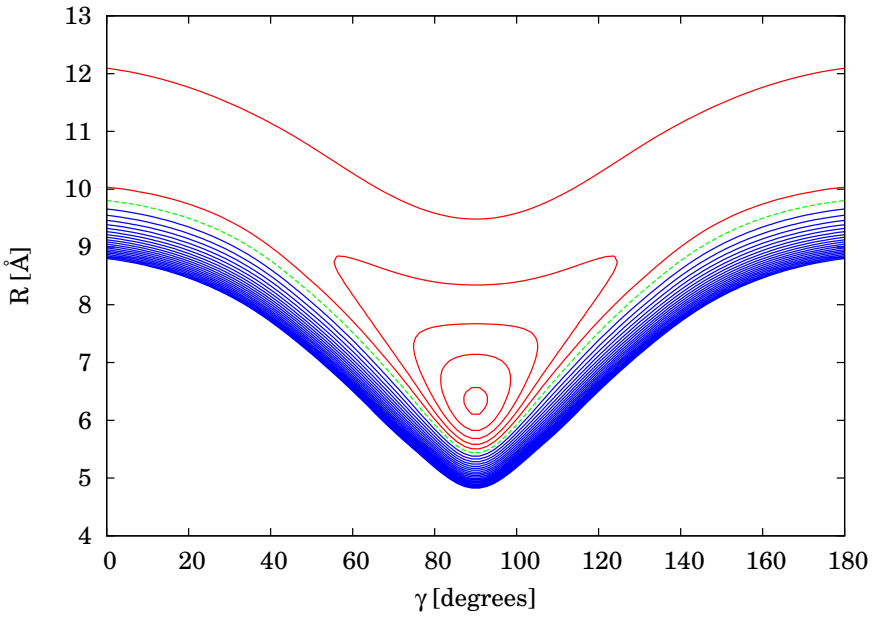

Figure 1: Equipotential contour lines of the potential energy of Rb_2He. The equipotential contours are in steps of 0.5 cm^{-1}. Red and blue contours correspond to negative and positive energies, respectively, and the green coutour (dashed) is the zero energy contour.

minimum of the potential corresponds to a T-shape geometry. It appears at a distance He-Rb_2

of 6.30 Å and has a depth of 2.59 cm^{-1}, which is in good agreement with the *ab initio* result mentioned above. The potential is attractive all around the Rb_2 diatomic molecule as emphasised by the red contour lines in Figure 1. However in the linear geometry, the system is bound by only -0.88 cm^{-1} at most. In order to assess the overall quality of the analytical potential, additional 104 *ab initio* energies randomly scattered in the spherical shell $R \in [5,25]$ Å and for which the potential is below 200 cm^{-1}, 10 cm^{-1}, and 0.1 cm^{-1} have been determined. The corresponding RMS errors of 0.49 cm^{-1}, 0.17 cm^{-1}, and 0.10 cm^{-1} underline the validity of the proposed global surface.

Monte Carlo study of Rb_2He_n

Description of the system and methods

The Rb_2He_N system is described using the cartesian coordinates of the helium atoms, of the Rb_2 center of mass, and the two angles giving the orientation of the diatomic principal axis. The resulting Hamiltonian is

$$\hat{H} = -\sum_{j}^{\mathscr{N}} D_j \frac{\partial^2}{\partial \mathscr{R}_j^2} + V(\mathscr{R}), \tag{3}$$

where $\mathscr{R}$ is a vector in the $\mathscr{N}$-dimensional space. $D_j = \hbar^2/2m_j$ if the j^{th} degree of freedom corresponds to a translation, and $D_j = B_0$ if this degree of freedom corresponds to a rotation. In the above equation, V is the potential between Rb_2 and He and between the He atoms. Since two rotations are allowed for the rigid linear rotor Rb_2, $\mathscr{N}$ is equal to $3N+5$. The potential interaction for the full cluster is evaluated using the pair potential approximation. In addition to the Rb_2-He potential we have developed, the He-He interaction potential of Aziz *et al.*[52] has been used. The rotational constant $B_0 = 0.01061$ $cm^{-1} = 0.0152$ K is computed using the geometry of Rb_2 and the mass $m_{Rb} = 84.91$ amu.

The Schrödinger equation is solved using the quantum diffusion[53–55] and path integral[56] Monte Carlo methods (DMC & PIMC). For DMC, the two rotational degrees of freedom are sampled as

explained in Ref. 57 using infinitesimal rotations of the principal axis frame of the Rb_2 rigid rotor. The implementation of DMC is done with a combination of weights and branching resulting in a constant ensemble size.[58,59] No guiding wave function has been used. For PIMC, we follow Ref. 56 and use the pair density approximation for the He-He interaction while using the simpler Trotter approximation for the Rb_2-He interaction. The implementation of rotational degrees of freedom in PIMC has been summarized in Ref. 60, and the application to linear molecules in ^{4}He nanodroplets can be found in Refs. 61,62.

The Rb_2He system

Given the exteme shallowness of the interaction potential, an additional study of the smallest cluster Rb_2He is done using an approach different from Monte Carlo simulation. The close coupling method is used to compute the rovibrational state of this van der Waals complex. For this study, the Jacobi coordinates R, γ are employed. The corresponding expression of the triatomic Hamiltonian, within the rigid rotor approximation for Rb_2 is

$$\hat{H} = -\frac{\hbar^2}{2\mu R}\frac{\partial^2}{\partial R^2}R + \frac{\hat{L}^2}{2\mu R^2} + B_0\hat{j}^2 + V^{\mathrm{Ak_2He}}(R,\gamma), \tag{4}$$

where μ is the Rb_2 - He reduced mass, $\hat{j}$ is the diatomic angular momentum and $\hat{L}$ is the orbital angular momentum describing the rotational motion of the He atom relative to the Rb_2 molecule. As in the Monte Carlo calculations, the spin-rotation and spin-spin coupling interactions of the diatomic molecule in the $^3\Sigma_u^+$ state have been neglected. The close coupled equations, identical to the ones arising in usual time-independent scattering calculations,[63,64] are solved with the appropriate bound state boundary conditions. The R-matrix propagator in the space-fixed reference frame, implemented in our close coupling code, is used. The method is found quite stable, and no stabilising transformations are needed. The detailed implementation of the method is found in Ref. 65.

The outward propagation, starting from the classically forbidden region and until R_{match} in the

region of the potential well, allows the computation of the R-matrix $R^{\text{out}}(R_{\text{match}})$ at this matching point. The inward propagation is done starting from the asymptotic region until R_{match} where the R-matrix is noted $R^{\text{in}}(R_{\text{match}})$. The eigenenergies of the system manifest themselves by a vanishing determinant of the difference $R^{\text{out}}(R_{\text{match}}) - R^{\text{in}}(R_{\text{match}})$.

Calculations are made for J, the quantum number related to the norm of the total angular momentum of the system, being equal to zero, so that results can be directly compared with those obtained with the DMC approach. Including 20 even rotational levels (ortho-states) from $j = 0$ to 38 in the diatomic basis and propagating from $R_{\text{min}} = 2$ Bohr to $R_{\text{match}} = 13$ Bohr outward and from $R_{\text{max}} = 100$ Bohr to R_{match} inward, a single bound state is found for the energy of -0.1927 K (e.g. -0.1339 cm^{-1}). The accuracy of this eigenenergy has been checked by varying both the sector size and R_{max}. For a given R_{max}, dividing the step size by a factor 2 does change the result by less than 2%. For the optimal step size, a reduction of R_{max} down to 50 Bohr does not affect the energy value by more than 0.1 %.

Quantum Monte Carlo studies of Rb_2He_N

We have simulated Rb_2He_N clusters for $N = 1,2,3,4,5,6,12$ and 20 using PIMC at low temperatures and DMC for up to $N = 5$. Due to the very weak attraction between Rb_2 and He, the stronger cumulative attraction among the He atoms leads to the formation of a cluster of the He atoms, to which the Rb_2 diatomic is weakly attached. Very low temperatures, $T = 1/25.6$ K for $N = 1,\ldots,6$, and $T = 1/6.4$ K for $N = 12,20$, have been used in the calculations in order to prevent evaporation of the weakly bound clusters.

Table 1 summarizes the total energies of the Rb_2He_N clusters and the chemical potential of ^{4}He, as obtained by PIMC and DMC simulations. For the PIMC results, we used a time step of $\Delta\tau = (40\text{K})^{-1}$, which is sufficiently small for the weak Rb_2-He interaction. The DMC results are extrapolated values with respect to both time step and ensemble size. The given associated error bars are estimated from the extrapolation procedure. The statistical error bars of each of the DMC computations, thus for a given time step and a given ensemble size, are found smaller than the

Table 1: Energies E_N [in K] and chemical potential $\mu_N[\mathrm{He}]$ [in K] of He for small Rb_2He_N clusters obtained by PIMC and DMC. The temperatures of the PIMC studies are $T = 1/25.6$ K for $N = 1-6$, and $T = 1/6.4$ K for $N = 12, 20$.

	PIMC		DMC	
N	E_N	$\mu_N[\mathrm{He}]$	E_N	$\mu_N[\mathrm{He}]$
0	0.0924	–	0.0	–
1	0.13 ± 0.06	-0.02 ± 0.06	-0.1929 ± 0.0004	-0.1929 ± 0.0004
2	-0.26 ± 0.02	-0.45 ± 0.09	-0.5623 ± 0.0009	-0.3694 ± 0.0013
3	-0.78 ± 0.04	-0.58 ± 0.06	-1.223 ± 0.006	-0.6607 ± 0.0069
4	-1.65 ± 0.05	-0.91 ± 0.09	-2.19 ± 0.01	-0.967 ± 0.016
5	-2.76 ± 0.03	-1.18 ± 0.08	-3.42 ± 0.09	-1.23 ± 0.1
6	-4.17 ± 0.10	-1.45 ± 0.13		
12	-15.74 ± 0.04	–		
20	-37.03 ± 0.05	–		

inaccuracy resulting from the extrapolations. We varied the time step from 800 a.u. (0.0025 K^{-1}) down to 50 a.u. (0.00016 K^{-1}) and the ensemble size up to 8000 walkers. For $N = 1$ there is perfect agreement between the DMC result and the result from the close coupling method mentioned above. The PIMC energies (second column) are consistently higher than the DMC ground state energies (fourth column), as expected at finite temperature. In particular the PIMC energy is positive for the bare Rb_2 molecule and the Rb_2He dimer, although the latter is bound. The third and fifth columns give the chemical potential for the He atoms for PIMC and DMC, respectively. The chemical potential μ_N is the difference between the energy of the Rb_2He_N cluster and the sum of energies of Rb_2He_{N-1} and a free He atom. At zero temperature, it is simply the difference $\mu_N[\mathrm{He}] \equiv E_N - E_{N-1}$, while at temperature T we have to take into account the thermal energy of the free He atoms, $\mu_N[\mathrm{He}] \equiv E_N - (E_{N-1} + \frac{3}{2}K_B T)$. $\mu_N[\mathrm{He}]$ decreases with N (i.e. the binding energy of an additional ^{4}He atom increases with N) slowly towards the bulk limit of -7.2K. Our comparison between PIMC and DMC in Table 1 shows that, despite large differences in total energies, $\mu_N[\mathrm{He}]$ is the same at zero temperature and at the temperature chosen for the small clusters – within the (fairly large) error bars of the PIMC result –, with the exception of the Rb_2He dimer. This means the calculation of the chemical potential is essentially unaffected by temperature.

From our PIMC calculations we computed the probability density $\rho_{\mathrm{Rb}_2}(r)$ to find the center of

mass of Rb_2 at a distance r from the center of mass of the He_N cluster. The densities are shown in Figure 2 for the cluster sizes studied. For $N = 1$, $\rho_{Rb_2}(r)$ is of course peaked at the average

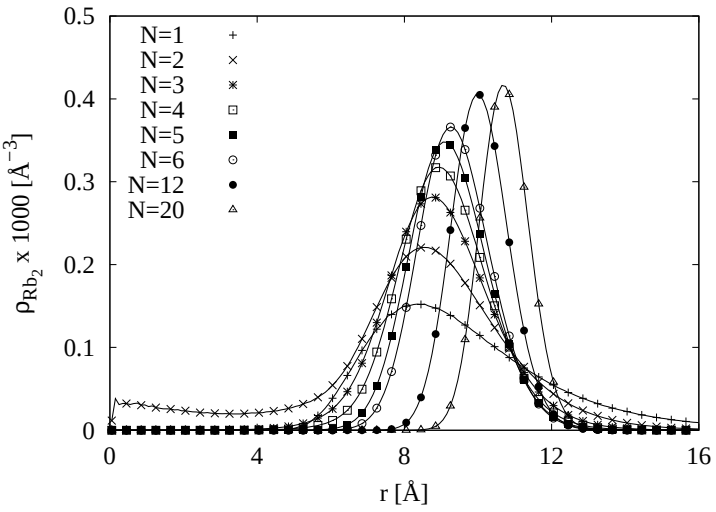

Figure 2: The probability density $\rho_{Rb_2}(r)$ to find the center of mass of Rb_2 at a distance r from the center of mass of the He_N cluster for $N = 1;2;3;4;5;6;12;20$. For $N = 1-6$, the temperature is $T = 1/25.6$ K, and for $N = 12$ and 20 $T = 1/6.4$ K.

distance between Rb_2 and He. Note that $\rho_{Rb_2}(r)$ falls off very slowly with $r \to \infty$, because of the low binding energy. For $N = 2$, we see that $\rho_{Rb_2}(r)$ is nonzero at $r = 0$, thus there is a finite probability that the two He atoms are on opposite sides of the center of mass of Rb_2. If, upon further increasing N, $\rho_{Rb_2}(r)$ developed a peak at $r = 0$, this would indicate that Rb_2 is solvated inside He_N. However, as expected from the weak Rb_2-He attraction, already for $N = 3$, $\rho_{Rb_2}(r)$ vanishes at $r = 0$ and presents a broad peak at a finite value of r. This means that the He atoms have zero probability to spread evenly around Rb_2, but rather cluster together. Upon further increasing N, the peak narrows and the position shifts to even larger r. This can be seen for $N = 20$, where the Rb_2 center of mass is well localized at about 11 Å from the center of mass of the $^4He_{20}$ cluster.

In Figure 3, we show a color map of the He density $\rho_{He}(r,z)$ in the coordinate frame defined by the center of mass of Rb_2 and the molecule axis as z-axis, for $N = 1-6, 12, 20$. The color encoding is logarithmic. With increasing N, the probability to find He atoms at the poles of Rb_2 indeed decreases, which is another indication that the He atoms cluster together, leaving Rb_2 on the "surface" of the cluster. The He_N cluster and Rb_2 are attached to each other such that the cluster

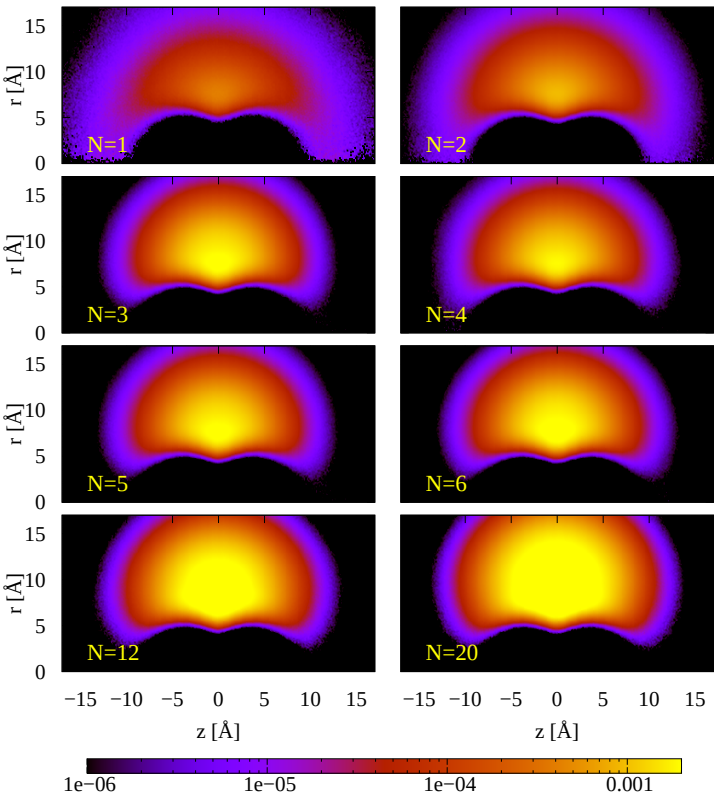

Figure 3: The He density $\rho_{\mathrm{He}}(r,z)$ in the coordinate frame defined by the center of mass of Rb_2 and the molecule axis as z-axis, for $N = 1-6, 12, 20$. For $N = 1-6$, the temperature is $T = 1/25.6$ K, and for $N = 12, 20$ $T = 1/6.4$ K.

resides as close as possible to the potential minimum. Thus, the Rb_2 axis and the line between the center of mass of Rb_2 and of He_N form a T shape. Extrapolating to the limit of large He droplets, as produced in experiments ($N = (10^3 - 10^4)$), the Rb_2 should swim on the surface of the droplet with its axis parallel to the surface. This is confirmed by simulations of Rb_2 on the flat surface of a He film in the following section.

In Ref. 16, Bovino *et al.* studied Li_2-He_N clusters for both the $^1\Sigma_g^+$ and the $^3\Sigma_u^+$ state of Li_2. In both cases, Li_2 was found to reside on the surface of the clusters, where $Li_2(^1\Sigma_g^+)$ favors an orientation perpendicular to the ^{4}He cluster surface and $Li_2(^3\Sigma_u^+)$ a parallel orientation. Although the translational and rotational zero-point motion of Li_2 is considerably larger than for Rb_2, the latter result is consistent with our result of a flat orientation for Rb_2 in the $^3\Sigma_u^+$ state. Although Li_2 is a homonuclear molecule with a corresponding symmetric interaction with ^{4}He, the ^{4}He

distribution around Li_2 was found to be *asymmetric* for $N = 20$. This is a notable difference to our results on Rb_2 where we see no evidence for such a peculiar asymmetry.

Rb_2 on a ^{4}He surface

We have performed PIMC simulations of Rb_2 on the surface of a He film, with the aim of an approximate representation of Rb_2 on the surface of a large He droplet, $N = O(10^3 - 10^4)$, as studied in experiments. The flat He film was simulated by 224 He atoms adsorbed on an artificial layer of solid He, at a temperature of $T = 1/3.2$K. In the two directions parallel to the film surface, periodic boundaries ($L \approx 28$Å) are applied, which implies about 4 "layers" of superfluid He. Since, due to the weak interaction with He, Rb_2 is adsorbed on the surface instead of being solvated by He, the layered structure of the He film (as opposed to the smooth density inside a He droplet) is not expected to greatly affect our results on structure and dynamics.

Structure

In Figure 4, we plot the angular probability distribution $\rho(\cos\theta)$ of the angle θ between the Rb_2 axis and the surface normal. The orientation of the Rb_2 axis is fluctuating around an orientation parallel to the surface, with zero probability for a perpendicular orientation. Therefore, a rotation of the molecule out of the surface is impossible for low rotational states, and pendular motion is the only relevant motion. Since the distribution $\rho(\cos\theta)$ is narrow around $\cos\theta = 0$, the orientational dynamics of Rb_2 can be approximated as the direct product of a planar 2D rotor mode and a pendular mode. We will discuss the dynamics of pendular motion and planar rotation further below.

Just like for adsorbed alkali atoms, the He density is deformed below the Rb_2 molecule: the adsorbed Rb_2 forms a dimple on the He surface. In Figure 5 we show the He density with respect to the center of mass and to the projection of the Rb_2 axis on the film plane. The figure shows a quarter of the dimple, the rest follows by reflection symmetry about the *xz* and *yz* planes. The He density is

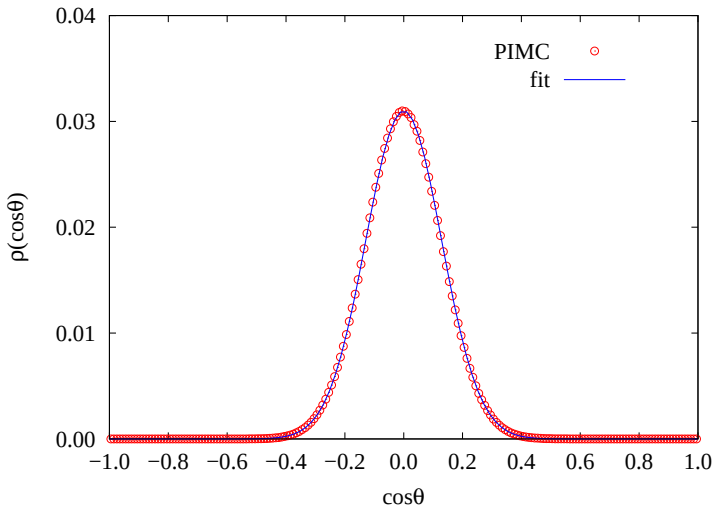

Figure 4: Angular distribution $\rho(\cos\theta)$ of the molecule axis of Rb_2 on a He surface. θ is defined with respect to the surface normal. The error bars are smaller than the symbols. The line is a Gaussian fit.

illustrated by a blue isosurface (at half the equilibrium density of bulk ^{4}He) as well as a color map of the density below in the *xz* and *yz* cut planes. The reference frame for the He density is defined by the Rb_2 location and orientation: the center of mass is situated at (0.,0.,0.), and the projection of the molecular axis on the plane of the surface defines the *x*-axis. Since Rb_2 is adsorbed with the molecule axis essentially parallel to the surface, the dimple is of course anisotropic, with two minima roughly below the two Rb atoms. This can be seen better in Figure 6, where we show the isosurface of the He density at half the equilibrium density of ^{4}He again, with additional color indicating the height of the isosurface in a quantitative manner. The two dimple minima are about 2.6Å deep, measured with respect to He surface further away from the Rb_2 molecule. This is to be compared to the average distance of the Rb_2 center of mass from the He surface which has a value of 3.8Å. This is larger than the depth of the dimple which means that the dimple is indeed shallow.

The density representation in Figure 5 contains also information about the density deep inside the He film, namely in the *xz* and *yz* planes. We see significant layering below the dimple, which is due to interaction with the wall adsorbing the ^{4}He film. Since these layers are well below the dimple, they will have only a small effect on Rb_2. In addition to this layering of the He film unrelated to Rb_2, there is a density increase right below the "waist" of the Rb_2 molecule in the

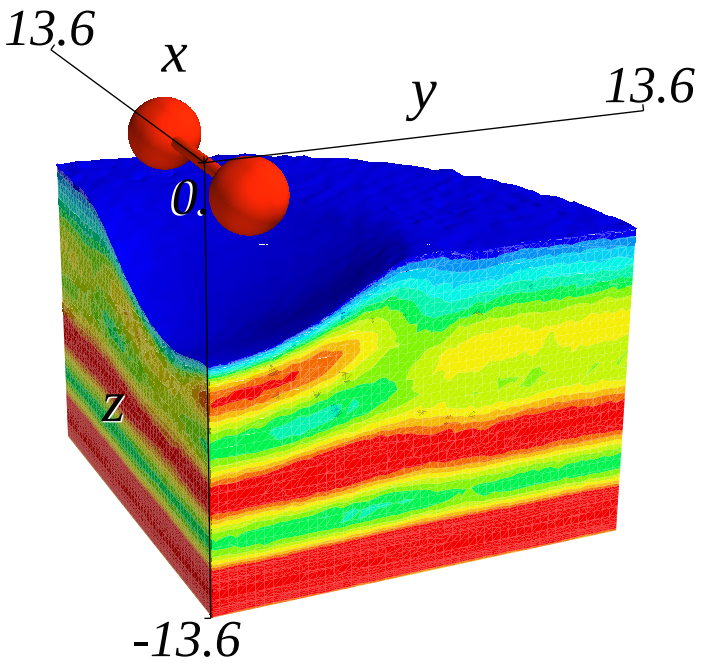

Figure 5: The figure shows a quarter of the anisotropic dimple in the He surface below Rb_2, the rest follows by reflection symmetry about the *xz* and *yz* planes. The He surface is illustrated by a blue isosurface, with the density shown in in the *xz* and *yz* cut planes (see text for details).

yz plane. There, the Rb_2-He interaction is strongest, attracting additional helium – but not strong enough to lead to full solvation of the molecule *inside* helium.

Dynamics

In the following three paragraphs we approximate the dynamics by assuming that the in-plane and out-of-plane rotations of Rb_2 are not coupled. As it will turn out that the excitation energies of the latter motion are by two order of magnitude larger than the former, this assumption makes indeed sense.

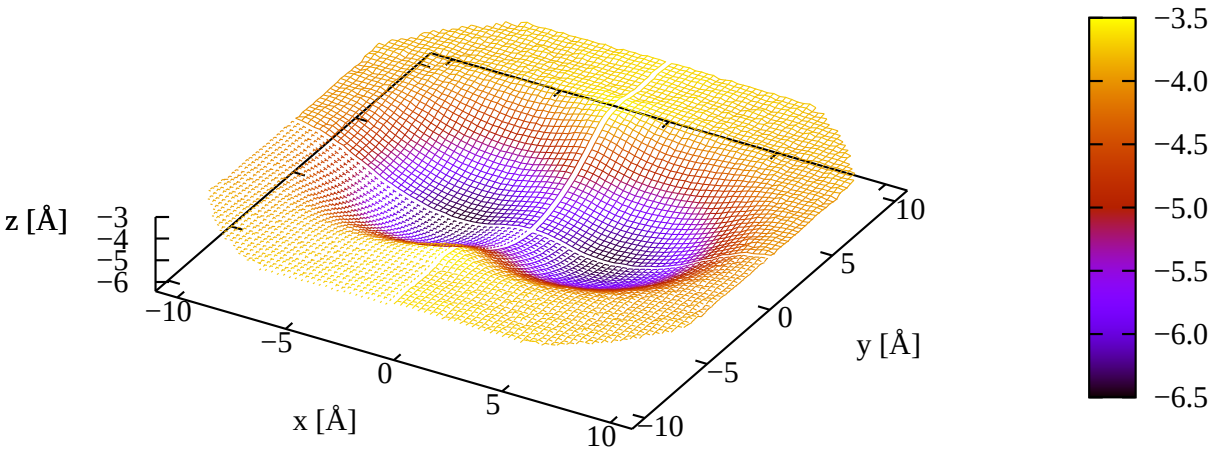

Figure 6: Isosurface of the He density relative to the Rb_2 molecule for half the equilibrium density $0.022/2$ Å^{-3}, with the Rb_2 center of mass at (0.,0.,0.).

Mean field approach: Pendular oscillations

We first treat the pendular motion in a mean field approach. This assumes that it can be described by an effective Hamiltonian

$$H_{\text{eff}} = B_0 \hat{L}^2 + V_H(\cos\theta) \tag{5}$$

where $\hat{L}$ is the angular momentum operator acting on the angle variable θ and ϕ of the molecule axis, and V_H is an effective static mean field potential generated by the He environment, which by symmetry is independent of ϕ.

Explicitely, H_{eff} is given by ($u \equiv \cos\theta$)

$$H_{\text{eff}} = -B_0 \Big(\frac{\partial}{\partial u}(1-u^2)\frac{\partial}{\partial u} + \frac{1}{1-u^2}\frac{\partial^2}{\partial \phi^2} \Big) + V_H(u). \tag{6}$$

The angular probability distribution $\rho(\cos\theta)$, see Figure 4, is localized around $u = \cos\theta = 0$, hence we assume $u^2 \ll 1$ and use the following approximation for H_{eff}

$$H_{\text{eff}} \approx -B_0 \frac{\partial^2}{\partial u^2} + V_H(u) - B_0 \frac{\partial^2}{\partial \phi^2} \tag{7}$$

which *decouples* the out-of-plane rotation associated with θ and the in-plane rotation associated

with ϕ. In the mean field approach the latter motion is free, leading to an effective rotational constant identical to the gas phase rotational constant. A better approximation to the in-plane rotation (still assuming decoupling, but exact otherwise) is used in the section below.

For small u, the mean field potential $V_H(u)$ can be approximated by $V_H(u) \approx au^2$, leading to harmonic pendular states for the out-of-plane rotation, *i.e.* Hermite polynomials. In particular the ground state is given by a Gaussian $\psi_0(u) \sim e^{-\alpha u^2}$, with $\alpha = \frac{1}{2}\sqrt{\frac{a}{B_0}}$. Indeed, we fitted a Gaussian $\psi_0^2(u) = e^{-2\alpha u^2}$ to $\rho(u)$ and obtained a virtually perfect fit, yielding $\alpha = 15.1$ ($\pm 0.1\%$), see also Figure 4. The resulting potential parameter is $a = 13.9$K. The ground state energy (zero point energy) is thus $E_0 = \frac{1}{2}\hbar\omega = \sqrt{aB_0} = 0.47$K, and the pendular excitation energies follow from $E_n - E_{n-1} = \hbar\omega = 0.94$K.

Full dynamics: Planar rotation

The above mean field approach would yield only the trivial approximation $B_{\text{eff}} = B_0$ for the planar rotational constant. Keeping the assumption of decoupled in-plane and out-of-plane rotations, we can improve on the estimate of B_{eff} by using the path integral correlation function (PICF) method, where we fit the imaginary time correlation function obtained by PIMC to the exact free 2D rotor correlation function, using B as a fitting parameter. We have employed this method for OCS in $^4\text{He}_N$ cluster and obtained good results for B_{eff}.[62]

The 2D rotor correlation function can be derived easily, because the exact wave function is known: $\langle\phi|m\rangle = \psi_m(\phi) = \frac{e^{im\phi}}{\sqrt{2\pi}}$, where $H|m\rangle = -B\frac{\partial^2}{\partial\phi^2}|m\rangle = Bm^2|m\rangle$. With the appropriate correlation operator $e^{iM\phi}$, we first define the associated spectral function

$$\begin{aligned} S_M(\omega) &= \frac{1}{Z}\sum_{mn}\delta(\hbar\omega - E_m + E_n)e^{-\beta E_n}|\langle m|e^{iM\phi}|n\rangle|^2 \\ &= \frac{1}{Z}\sum_{n}\delta(\hbar\omega - B(M+n)^2 + Bn^2)e^{-\beta Bn^2}\ , \end{aligned} \tag{8}$$

with $Z = \sum_n e^{-\beta Bn^2}$. $S_M(\omega)$ cannot be sampled directly with PIMC, but its Laplace transform can

be sampled:

$$F_M(\tau) = \int_{-\infty}^{\infty} d\omega e^{-\omega\tau} S_M(\omega) = \frac{1}{Z}\sum_n e^{-B(M+n)^2\tau} e^{-Bn^2(\beta-\tau)}. \tag{9}$$

$F_M(\tau)$ can be calculated by bringing it into the following form

$$F_M(\tau) = \frac{1}{Z}\mathrm{Tr}\left\{e^{iM(\phi(\tau)-\phi(0))}e^{-\beta H}\right\} \tag{10}$$

which can be trivially sampled by PIMC.

In Figure 7 we plot the imaginary time correlation function $F_M(\tau)$ for the lowest angular momentum quantum number $M = 1$, from $\tau = 0$ to $\tau = \beta/2$. The free 2D rotor fit yielding an effective

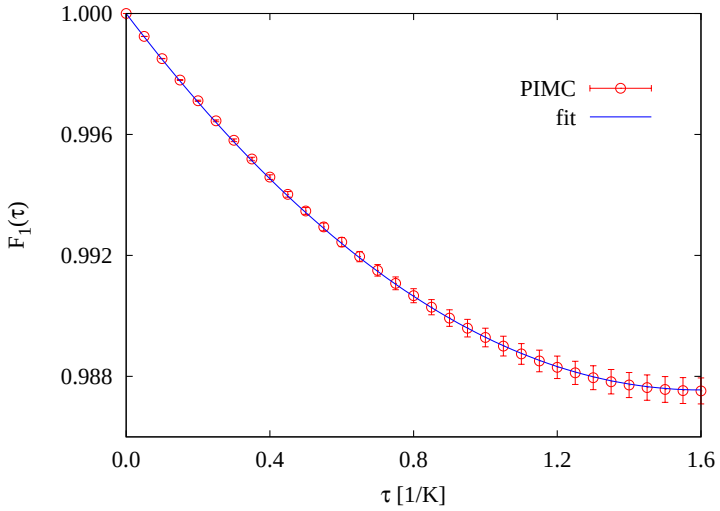

Figure 7: Correlation function $F_1(\tau)$ and free 2D rotor fit yielding an effective rotational constant B_{eff}. Its value is 103%±3% of the gas phase value B_0, *i.e.* indistinguishable from B_0. For better visibility, only every other PIMC data point is plotted.

rotational constant B_{eff} is also shown. The fitted B_{eff} value is 103%±3% of the gas phase value B_0, *i.e.* indistinguishable from B_0 within the error bar. Fitting to $F_M(\tau)$ for $M = 2,\ldots,5$ gives the same result. This means that Rb_2 rotates almost freely in the film plane, with only weak coupling to surface excitations (ripplons) of the He film. Hence the rotational dynamics of the heavy rotor Rb_2 on the surface of helium is very different from the dynamics of heavy rotors solvated inside helium, where a reduction to only 20-40% of the gas phase value is found.[3] Information about the coupling of adsorbed molecules like Rb_2 with surface excitations could be extracted by study-

ing decay mechanism, leading to a homogeneous linewidth, but such detailed information about rotational spectra cannot be obtained by PIMC.

Full dynamics: Pendular oscillations

As for the in-plane rotation, we use the PICF method to calculate the excitation energies of the pendular states including dynamic coupling between Rb_2 and the He film as opposed to the mean field approach above. For that purpose we sample a suitable correlation function. The resulting correlation function is fitted by the corresponding correlation function of the harmonic oscillator. We expect changes from the mean field result, due to a *perpendicular* effective moment of inertia due to the dynamic response of the helium.

The pendular term of the approximate effective Hamiltonian $H_{\rm eff}$ Eq. (5) is equivalent to a 1D harmonic oscillator. Hence we need to calculate an appropriate correlation function $F(t)$ in imaginary time. The parameters to be fitted to the PICF are the rotational constant B and the potential parameter a.

The Hamiltonian of a particle of mass $\mathscr{M}$ in a one-dimensional harmonic oscillator potential of frequency ω is

$$H = \frac{\bar{h}^2}{2\mathscr{M}}\frac{d^2}{du^2} + \frac{1}{2}\mathscr{M}\omega^2 u^2. \tag{11}$$

Comparing with the effective pendular Hamiltonian in the approximation of small pendular oscillations, Eq. (7), we can therefore associate

$$B \equiv \frac{\bar{h}^2}{2\mathscr{M}}, \qquad a \equiv \frac{1}{2}\mathscr{M}\omega^2, \tag{12}$$

hence

$$\bar{h}\omega = 2\sqrt{aB}. \tag{13}$$

We choose the auto-correlation function of the coordinate $u = \cos\theta$

$$F(\tau) = \langle u(\tau)u(0)\rangle_\beta = \frac{1}{Z}\mathrm{Tr}\{u(\tau)u(0)e^{-\beta H}\}. \tag{14}$$

We calculate the trace in the basis of the harmonic oscillator states $|n\rangle$. The canonical partition function is

$$Z = \mathrm{Tr}\{e^{-\beta H}\} = \frac{e^{-\beta\hbar\omega/2}}{1-e^{-\beta\hbar\omega}}. \tag{15}$$

We express u in terms of the creation and annihilation operator of harmonic oscillator states to obtain the matrix elements needed for calculating $F(\tau)$,

$$\begin{aligned} F(\tau) &= \frac{1}{Z}\sum_{n,m} |\langle n|x|m\rangle|^2 e^{-\tau\hbar\omega(m+1/2)} e^{-(\beta-\tau)\hbar\omega(n+1/2)} \\ &= \frac{1}{Z}\frac{B}{\hbar\omega}\sum_n e^{-\beta\hbar\omega(n+1/2)}\Big[(n+1)e^{-\tau\hbar\omega} + ne^{+\tau\hbar\omega}\Big]. \end{aligned} \tag{16}$$

The (derivatives of) the geometric sums can be evaluated to obtain the simple analytical expression

$$F(\tau) = B\frac{1}{\hbar\omega}\frac{e^{-(\beta-\tau)\hbar\omega} + e^{-\tau\hbar\omega}}{1-e^{-\beta\hbar\omega}}. \tag{17}$$

The parameters $\hbar\omega$ and B appearing in $F(\tau)$, Eq. (17), can now be obtained by fitting to the exact auto-correlation function $F(\tau)$ which we sample by PIMC.

In Figure 8, we plot $F(\tau)$ obtained by PIMC (symbols) and the effective free harmonic oscillator fit (full line). The fit yields a reduced effective rotational constant $B = B_{\mathrm{eff}}$ for the pendular motion, with a value of 87% of the gas phase value B_0. The fitted oscillator frequency is $\hbar\omega = 0.89$K, which is slightly lower than the value 0.94K obtained by the mean field approach above. For comparison, we also show $F(\tau)$ with the parameters obtained in mean field approximation (dashed line), which has only qualitatively the right shape, but does not agree quantitatively with the exact $F(\tau)$ from PIMC.

Superfluidity and Bose-Einstein condensation

At the temperature of our PIMC simulations, $T = 0.31$K, ^{4}He is essentially 100% superfluid if not perturbed by the interaction with the adsorbed Rb_2 molecule. Note that the same applies for the interaction due to the wall, which is not the focus of this work. The suppression of superfluidity

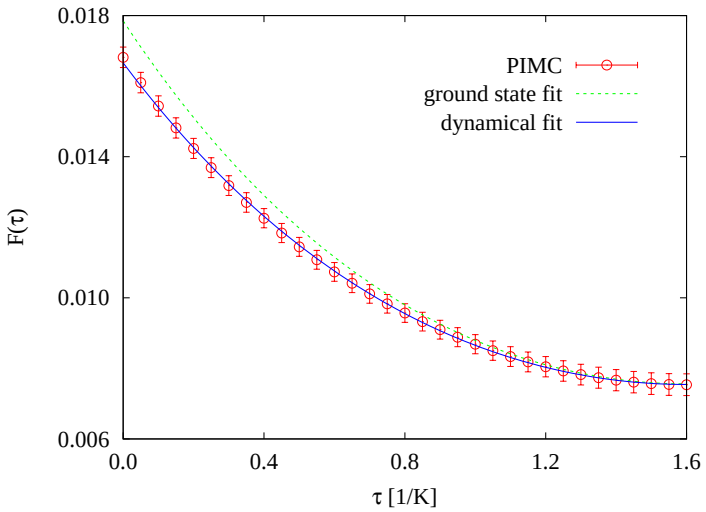

Figure 8: Correlation function $F(\tau)$ obtained by PIMC (symbols) and the free HO fit (blue line) yielding a reduced effective rotational constant B_{eff} for the *pendular* motion. For comparison, $F(\tau)$ computed with the parameters obtained in mean field approximation (green dashed line) is also shown. For better visibility, only every other PIMC data point is plotted.

of ^{4}He close to molecules inside ^{4}He nanodroplets has been actively investigated by PIMC simulations.[66,67] The concept of the local nonsuperfluid fraction adiabatically following the molecule rotation permits to quantitatively account for the increase of the effective moment of inertia for heavy molecules. The local superfluid density is calculated by a coordinate-dependent area estimator.[68] The local nonsuperfluid density is obtained by subtraction of this local superfluid density from the total density. In the present case, one can expect that the superfluid fraction for a rotation axis perpendicular to the surface is only slightly suppressed below the Rb_2 molecule, because the Rb_2-He interaction is weak. The nonsuperfluid density is therefore a small quantity resulting from the difference of two large numbers, both of them afflicted by stochastic noise from the PIMC simulation. Furthermore, due to the position of the molecule on the surface of ^{4}He rather than at the center of the droplet, arguments based on rotational symmetry of linear rotors cannot be used to lower the computational cost. Instead we would have to sample the local superfluidity in all three dimensions. The area estimator is subject to large stochastic noise, which would be amplified by orders of magnitude by three dimensional binning. In conclusion, we doubt that the probably small local nonsuperfluid fraction below the Rb_2 can be obtained in reasonable simulation times.

A more appropriate starting point for the study of the local nonsuperfluid fraction induced by a surface adsorbed dopant would be a particle of spherical symmetry, e.g. an alkali atom. Furthermore, it would be favorable to have a steep dimple rather than a shallow one, since the nonsuperfluid fraction would be larger.

The notion of Bose-Einstein condensation is usually not invoked in the field of spectroscopy of doped ^{4}He nanodroplets. Nevertheless, the expected modification of the condensate fraction by an adsorbed particle on ^{4}He is an interesting question. The condensate fraction is only 7-8% in bulk ^{4}He due to condensate depletion by the He-He interactions. However, as we move away from the surface towards the vacuum side, the condenstate fraction tends towards 100% because ^{4}He becomes more and more dilute (less interaction). An adsorbed particle like the Rb_2 molecule increases the interaction for ^{4}He atoms below the adsorbant, thus this should lead to a local depletion of the surface condensate. As for the local nonsuperfluid fraction below the adsorbant, a spherical particle would be a more appropriate starting point to study the depletion effect.

Conclusions

Superfluid helium nanodroplets have become a unique tool for low temperature matrix spectroscopy of isolated atoms and molecules, and of molecular complexes. Helium nanodroplet isolation spectroscopy has made possible numerous high resolution spectroscopic studies of the high-spin alkali dimers bringing valuable insight into their properties at the microscopic level.

In this work, a study of Rb_2 in its ground triplet state in a weakly perturbing environment of superfluid ^{4}He has been presented. We have neglected the vibrational motion of the Rb_2 molecule, treating the molecule as a rigid rotor. A study of small Rb_2He_N clusters showed an agglomeration of the He atoms to a cluster and a localization of Rb_2 outside of the He cluster. In addition, we found a parallel orientation of Rb_2 with respect to the surface of the helium cluster. This orientation is confirmed in a further study of Rb_2 on the surface of an infinite helium film taken as

an approximation to the surface of a large He droplet of thousands of He atoms, as typically used in experiments. Analysis of the He density relative to Rb_2 shows that even in the limit of a flat surface, only a shallow (anisotropic) dimple forms in the He film below the Rb_2 molecule, with a maximum depth of only 2.6Å. The rotational dynamics of Rb_2 on a helium surface indicate that the in-plane rotation is weakly perturbed by the He surface. Conversely, the out-of-plane rotation is completely hindered, allowing only pendular motion of the Rb_2 molecule that is well approximated by harmonic oscillator modes with a frequency of $\hbar\omega = 0.89$K, similar to the result of a simpler mean field treatment.

These studies are done using a completely new potential energy surface, calculated at the *ab initio* level using the CCSD(T) method, with a recent effective core potential for the rubidium atom. The analytic representation of the potential, implemented using the RKHS method, is found to reproduce well the *ab initio* data.

In addition to the Monte Carlo calculations, the bound states of the smallest cluster, Rb_2He, have been determined with the close coupling method. The energy obtained for the unique bound state of this van der Waals complex is found to be in good agreement with the DMC result.

In the future, several important points deserve to be studied. First of all, the vibration of Rb_2 should be taken into account. A full 3-dimensional potential energy surface is currently under construction in our group. Such a surface is a mandatory first step to provide a theoretical insight of the recent experimental results on the decoherence of vibrationally excited alkali dimers on the surface of helium droplets.[15,19,20,69] Secondly, the spin statistics, entirely neglected here, along with the fine structure of Rb_2 in triplet states could play an important role. The question of possible effects of helium atoms on the fine structure constants could then be addressed. On the longer term, the question of electronic excitations of Rb_2 could be looked at. However, the accurate calculation of electronically excited states of such an heavy alkali dimer remains itself a considerable challenge which is increased by the need to represent the weak interaction with helium atoms. Still the presence of many crossings and non adiabatic couplings between these excited electronic states could be the ground of spectroscopic and dynamical subtleties.

Acknowledgments

This work is supported by the Région Bretagne via the project CREATE “4023-HELIUM”, by Egide via the Amadeus (Amadée) PHC program # 17283PE (FR 14/2008) and via the project ANR “DYNHELIUM”. M.L. acknowledges grants from CNRS and from the Academy of Finland. R.E. Zillich thanks the University of Rennes 1 for financial support of an extended visit in Rennes. We thank Wolfgang Ernst and Marcel Mudrich for interesting discussions.

References

[1] Toennies, J. P.; Vilesov, A. F.; Whaley, K. B. *Physics Today* **2001**, *54*, 31–36.

[2] Grebenev, S.; Toennies, J. P.; Vilesov, A. F. *Science* **1998**, *279*, 2083–2086.

[3] Toennies, J. P.; Vilesov, A. F. *Angew. Chem. Int. Ed.* **2004**, *43*, 2622–2648.

[4] Ancilotto, F.; Cole, M. W.; DeToffol, G.; Lerner, P. B.; Toigo, F. *J. Low Temp. Phys.* **1995**, *101*, 325–330.

[5] Lerner, P. B.; Cole, M. W.; Cheng, E. *J. Low Temp. Phys.* **1995**, *100*, 501–514.

[6] Stienkemeier, F.; Ernst, W.; Higgins, J.; Scoles, G. *J. Chem. Phys.* **1995**, *102*, 615–617.

[7] Higgins, J.; Callegari, C.; Reho, J.; Stienkemeier, F.; Ernst, W. E.; Gutowski, M.; Scoles, G. *J. Phys. Chem. A* **1998**, *102*, 4952–4965.

[8] Brühl, F. R.; Miron, R. A.; Ernst, W. E. *J. Chem. Phys.* **2001**, *115*, 10275–10281.

[9] Bodo, E.; Gianturco, F. A.; Yurtsever, E.; Yurtsever, M. *Mol. Phys.* **2005**, *103*, 3223–3231.

[10] Allard, O.; Nagl, J.; Auböck, G.; Callegari, C.; Ernst, W. E. *J. Phys. B* **2006**, *39*, S1169–S1181.

[11] Claas, P.; Droppelmann, G.; Schulz, C. P.; Mudrich, M.; Stienkemeier, F. *J. Phys. B* **2006**, *39*, S1151–S1168.

[12] Ernst, W. E.; Huber, R.; Jiang, S.; Beuc, R.; Movre, M.; Pichler, G. *J. Chem. Phys.* **2006**, *124*, 024313–1–6.

[13] Auböck, G.; Nagl, J.; Callegari, C.; Ernst, W. E. *J. Phys. Chem. A* **2007**, *111*, 7404–7410.

[14] Claas, P.; Droppelmann, G.; Schulz, C. P.; Mudrich, M.; Stienkemeier, F. *J. Phys. Chem. A* **2007**, *111*, 7537–7541.

[15] Nagl, J.; Auböck, G.; Callegari, C.; Ernst, W. E. *Phys. Rev. Lett.* **2007**, *98*, 075301–1–4.

[16] Bovino, S.; Coccia, E.; Bodo, E.; Lopez-Drán, D.; Gianturco, F. A. *J. Chem. Phys.* **2009**, *130*, 224903–1–9.

[17] Mudrich, M.; Heister, P.; Hippler, T.; Giese, C.; Dulieu, O.; Stienkemeier, F. *Phys. Rev. A* **2009**, *80*, 042512–1–12.

[18] Prosmiti, R.; Delgado-Barrio, G.; Villarreal, P.; Yurtsever, E.; Coccia, E.; Gianturco, F. A. *J. Phys. Chem. A* **2009**, *113*, 14718–14729.

[19] Auböck, G.; Aymar, M.; Dulieu, O.; Ernst, W. E. *J. Chem. Phys.* **2010**, *132*, 054304–1–7.

[20] Schlesinger, M.; Mudrich, M.; Stienkemeier, F.; Strunz, W. *Chem. Phys. Letters* **2010**, *490*, 245–248.

[21] Vongehr, S.; Kresin, V. V. *J. Chem. Phys.* **2003**, *119*, 11124–11129.

[22] Schulz, C. P.; Claas, P.; Schumacher, D.; Stienkemeier, F. *Phys. Rev. Lett.* **2004**, *92*, 013401–1–4.

[23] Amiot, C.; Crozet, P.; Vergès, J. *Chem. Phys. Letters* **1985**, *121*, 390–394.

[24] Amiot, C. *Mol. Phys.* **1986**, *58*, 667–687.

[25] Amiot, C. *J. Chem. Phys.* **1990**, *93*, 8591–8604.

[26] Amiot, C. *Chem. Phys. Letters* **1995**, *241*, 133–139.

[27] Amiot, C.; Vergès, J. *Chem. Phys. Letters* **1997**, *274*, 91–98.

[28] Anderson, M. H.; Ensher, J. R.; Matthews, M. R.; Wieman, C. E.; Cornell, E. A. *Science* **1995**, *269*, 198–201.

[29] Bradley, C. C.; Sackett, C. A.; Tollett, J. J.; Hule, R. G. *Phys. Rev. Lett.* **1995**, *75*, 1687–1690.

[30] Davis, K. B.; Mewes, M. O.; Andrews, M. R.; van Druten, N. J.; Durfee, D. S.; Kurn, D. M.; Ketterle, W. *Phys. Rev. Lett.* **1995**, *75*, 3969–3973.

[31] Miller, J. D.; Cline, R. A.; Heinzen, D. J. *Phys. Rev. Lett.* **1993**, *71*, 2204–2207.

[32] Cline, R. A.; Miller, J. D.; Heinzen, D. J. *Phys. Rev. Lett.* **1994**, *73*, 632–635.

[33] Gardner, J. R.; Cline, R. A.; Miller, J. D.; Heinzen, D. J.; Boesten, H. M. J. M.; Verhaar, B. J. *Phys. Rev. Lett.* **1995**, *74*, 3764–3767.

[34] Tsai, C. C.; Freeland, R. S.; Vogels, J. M.; Boesten, H. M. J. M.; Verhaar, B. J.; Heinzen, D. J. *Phys. Rev. Lett.* **1997**, *79*, 1245–1248.

[35] Lang, F.; Winkler, K.; Strauss, C.; Grimm, R.; Denschlag, J. H. *Phys. Rev. Lett.* **2008**, *101*, 133005–1–4.

[36] Weiner, J.; Bagnato, V. S.; Zilio, S.; Julienne, P. S. *Rev. Mod. Phys.* **1999**, *71*, 1–85.

[37] Spiegelmann, F.; Pavolini, D.; Daudey, J. *J. Phys. B* **1989**, *22*, 2465–2483.

[38] Krauss, M.; Stevens, W. J. *J. Chem. Phys.* **1990**, *93*, 4236–4242.

[39] Foucrault, M.; Millie, P.; Daudey, J. P. *J. Chem. Phys.* **1991**, *93*, 1257–1264.

[40] Lozeille, J.; Fioretti, A.; Gabbanini, C.; Huang, Y.; Pechkis, H. K.; Wang, D.; Gould, P. L.; Eyler, E. E.; Stwalley, W.; Aymar, M.; Dulieu, O. *Eur. Phys. J. D.* **2006**, *39*, 261–269.

[41] Kotochigova, S.; Tiesinga, E.; Julienne, P. S. *Phys. Rev. A* **2000**, *63*, 012517–1–4.

[42] Soldán, P. *J. Chem. Phys.* **2010**, *132*, 234308–1–7.

[43] Strauss, C.; Takekoshi, T.; Lang, F.; Winkler, K.; Grimm, R.; Denschlag, J. H.; Tiemann, E. *Phys. Rev. A* **2010**, *82*, 052514–1–12.

[44] Pascale, J. *Phys. Rev. A* **1983**, *28*, 632–644.

[45] Kleinekathöfer, U.; Tang, K. T.; Toennies, J. P.; Yiu, C. L. *Chem. Phys. Letters* **1996**, *249*, 257–263.

[46] Zbiri, M.; Daul, C. *J. Chem. Phys.* **2004**, *121*, 11625–11628.

[47] Boys, S. F.; Bernardi, F. *Mol. Phys.* **1970**, *19*, 553–566.

[48] Amos, R. D. et al. MOLPRO, a package of ab initio programs designed by H.-J. Werner and P. J. Knowles, version 2002.1. 2002.

[49] Lim, I. S.; Schwerdtfeger, P.; Metz, B.; Stoll, H. *J. Chem. Phys.* **2005**, *122*, 104103–1–12.

[50] Beser, B.; Sovkov, V. B.; Bai, J.; Ahmed, E. H.; Tsai, C. C.; Xie, F.; Li, L.; Ivanov, V. S.; Lyyra, A. M. *J. Chem. Phys.* **2009**, *131*, 094505–1–6.

[51] Ho, T. S.; Rabitz, H. *J. Chem. Phys.* **1996**, *104*, 2584–2597.

[52] Aziz, R. A.; McCourt, F. R. W.; Wong, C. C. K. *Mol. Phys.* **1987**, *61*, 1487–1511.

[53] Reynolds, P. J.; Ceperley, D. M.; Alder, B. J.; Lester, W. A. *J. Chem. Phys.* **1982**, *77*, 5593–5603.

[54] Suhm, M. A.; Watts, R. O. *Phys. Rep.* **1991**, *204*, 293–329.

[55] Buch, V. *J. Chem. Phys.* **1992**, *97*, 726–729.

[56] Ceperley, D. M. *Rev. Mod. Phys.* **1995**, *67*, 279–355.

[57] Viel, A.; Patel, M. V.; Niyaz, P.; Whaley, K. B. *Comp. Phys. Com.* **2002**, *145*, 24–47.

[58] Blume, D.; Lewerenz, M.; Huisken, F.; Kaloudis, M. *J. Chem. Phys.* **1996**, *105*, 8666–8883.

[59] Viel, A.; Coutinho-Neto, M. D.; Manthe, U. *J. Chem. Phys.* **2007**, *126*, 024308–1–9.

[60] Marx, D.; Müser, M. U. *J. Phys.: Condens. Matter* **1999**, *11*, 117–155.

[61] Blinov, N.; Song, X.; Roy, P. N. *J. Chem. Phys.* **2004**, *120*, 5916–5931.

[62] Zillich, R. E.; Paesani, F.; Kwon, Y.; Whaley, K. B. *J. Chem. Phys.* **2005**, *123*, 114301–1–12.

[63] Arthurs, A. M.; Dalgarno, A. *Proc. Roy. Soc. A* **1961**, *256*, 540–551.

[64] Pack, R. T. *J. Chem. Phys.* **1974**, *60*, 633–639.

[65] Danby, G. *J. Phys. B* **1983**, *16*, 3393–3410.

[66] Kwon, Y.; Whaley, K. B. *J. Chem. Phys.* **2001**, *115*, 10146–10153.

[67] Paesani, F.; Kwon, Y.; Whaley, K. B. *Phys. Rev. Lett.* **2005**, *94*, 153401–1–4.

[68] Kwon, Y.; Paesani, F.; Whaley, K. B. *Phys. Rev. B* **2006**, *74*, 174522–1–10.

[69] Grüner, B.; Schlesinger, M.; Heister, P.; Strunz, W. T.; Stienkemeier, F.; Mudrich, M. **2010**, arXiv:1011.0924.